Supporting Information

Achievement of High-Level Reverse Intersystem Crossing in Rubrene-Doped Organic Light-Emitting diodes

Xiantong Tang,[†] *Ruiheng Pan,*[‡] *Xi Zhao,*[†] *Hongqiang Zhu,*[§] *and Zuhong Xiong*[*,†]

[†]*School of Physical Science and Technology, MOE Key Laboratory on Luminescence and Real-Time Analysis, Southwest University, Chongqing 400715, China*

[‡]*Key Laboratory of Luminescence and Optical Information, Ministry of Education, School of Science, Beijing Jiaotong University, Beijing 100044, China*

[§]*Chongqing Key Laboratory of Photo-Electric Functional Materials, Chongqing Normal University, Chongqing 401331, China*

Corresponding Authors:

zhxiong@swu.edu.cn

Supporting Text S1:

Under electrical pumping, exciton formation of the dopant (or guest) in a doped (host-guest) system can occur either through direct charge trap (DCT) or by energy transfer (ET) mechanisms.[1] The former denotes that the injected carriers can directly form excited states on guest molecules, whereas guest excitons have to overcome highest occupied molecular orbital (HOMO) and lowest unoccupied molecular orbital (LUMO) energy barriers ($\Delta E_{\text{HOMO-HOMO}}$ and $\Delta E_{\text{LUMO-LUMO}}$) through thermal activation or tunneling processes to diffuse.[2] By contrast, the latter refers to that guest molecules cannot directly capture carriers but rather accept energy released from host excitons through Förster resonance or Dexter energy transfer (FRET and DET) mechanisms to form guest excitons.[1] FRET only occurs between singlet excitons of host and guest and depends on the overlap of the host emission spectrum and guest absorption spectrum.[3] DET mainly occurs between the triplet excitons of the host and guest.[4] Generally, a smaller difference between the triplet energy levels of the host and guest yields more efficient DET processes.[5] On the whole, formation of excitons by ET must compete with that by DCT mechanism, and these two mechanisms have significant effects on the performance of the devices.

Supporting Text S2:

Based on the analysis of Figure 2a in our main manuscript, under any specific bias currents, the low-field effects of the MEL curves (MEL_{LFE}) are solely determined by the HL-RISC process and their corresponding magnitudes are displayed in Figure 2e. The high-field effects of the MEL curves (MEL_{HFE}) depend on SF or TF processes, and their current-dependent magnitudes determined by the comprehensive effects of SF and TF processes are depicted in

the inset of Figure 2e. Clearly, it is difficult to precisely distinguish the proportion of SF and TF processes at a specific bias current due to their highly correlated relationship of these two processes. To approximately pinpoint the main/dominant processes under a fixed current, it is necessary for us to make the following assumptions: SF (TF) should only be considered when the magnitude of MEL_{HFE} is positive (negative), and as presented in Figure 2e their corresponding bias currents are smaller (larger) than 300 μA, respectively. Thus, the relative proportions of these three physical mechanisms (including HL-RISC, TF, and SF) can be reflected by the contribution ratio [$R_{LFE(HFE)}$] of their corresponding MEL_{LFE} and MEL_{HFE} values, which can be expressed as:

$$R_{LFE(HFE)} = \frac{|MEL_{LFE(HFE)}|}{|MEL_{LFE}| + |MEL_{HFE}|} \times 100\% \quad \text{(S1)}$$

where the MEL_{LFE} and MEL_{HFE} values at different bias currents can be obtained from Figure 2e and its inset, respectively. According to this formula, the contribution ratios of each microscopic process under different bias currents are calculated and shown in Figure S3.

Supporting Text S3:

Regrettably, we cannot directly provide the external-quantum-efficiency (EQE)-current-density (*J*) curves at various temperatures to detect whether the efficiency of our rubrene-based OLEDs will be further improved due to the enhanced HL-RISC by lowering the operational temperature or not. This is because the current experimental equipment in our Lab cannot test the accurate brightness values of OLEDs at low- or high-temperature measurement environments. Thus, we add the relative temperature-dependent luminance(*L*)-current (*I*) characteristic curves (Figure S6, here the luminance is measured by

a Si photo-detector) to supporting information for indirectly reflecting the improved efficiency of our OLEDs at low operational temperatures. According to the literature,[6] Okamoto et al. proposed a very simple method of calculating the external quantum efficiency (η_{EQE}) of OLEDs, and η_{EQE} can be expressed via using the following formula:

$$\eta_{EQE} = \frac{\pi e}{683hc} \times \frac{\int_{380}^{780} I(\lambda)\lambda d\lambda}{\int_{380}^{780} I(\lambda)K(\lambda)d\lambda} \times \frac{L}{I} \quad \text{(S2)}$$

where e is the elementary charge of electron, h is the Planck's constant, c is the velocity of light, $K(\lambda)$ is the Commission International de l'Eclairage chromaticity standard photopic efficiency function, $I(\lambda)$ is the relative electroluminescence (EL) intensity at each wavelength obtained from the measurement of EL spectrum, L is the luminance, and I is the current. According to eq. S2, η_{EQE} is mainly related to three factors, including EL spectrum, luminance, and current. When the EL spectra of devices at various temperatures are the same and the current through the device is fixed, η_{EQE} is proportional to the luminance intensity and can be expressed as:

$$\eta_{EQE} \propto kL \quad \text{(S3)}$$

where k is a coefficient mainly related to the EL spectrum and the current.

Supporting Text S4:

DCT mechanism only can dominate at high dopant concentration, because the small molecular space distance between guest molecules is necessary for the formation of polaron pair states in rubrene ($PP_{1,\ rub}$ and $PP_{3,\ rub}$). The specific analysis is as follows: In terms of DCT-dominated OLEDs (Figure S7), under electrical excitation, 25% of the $PP_{1,\ rub}$ and 75% of $PP_{3,\ rub}$ in rubrene molecules are initially created. These polaron pairs subsequently form

corresponding $S_{1,\,rub}$ and $T_{1,\,rub}$ states under the interaction of Coulomb attraction rather than undergo an ISC process ($PP_{1,\,rub} \rightarrow PP_{3,\,rub}$), which only can be observed under high bias currents.[5] Thereafter, as discussed above, the deactivation of $S_{1,\,rub}$ states can proceed through a prompt fluorescence [channel ①] to ground states, or via an ultrafast spin-dependent SF process to create $T_{1,\,rub}$ states, which can generate delayed fluorescence [channel ②] by a TF process. Therefore, it is noteworthy that $T_{2,\,rub}$ excitons cannot form under this circumstance, which is responsible for the absence of HL-RISC process in DCT-dominated OLEDs.

Supporting Table:

Emissive layer	V_{on} (V)	Maximal Luminance (cd/m^2)	Maximal EQE (%)
CBP: 10%rubrene	3.2	4066	5.22
Pure rubrene	4.0	656	0.55

Table R1. Performance data of 10%rubrene-doped and pure-rubrene devices extracted from Figure 1d,S2.

Supporting Figures:

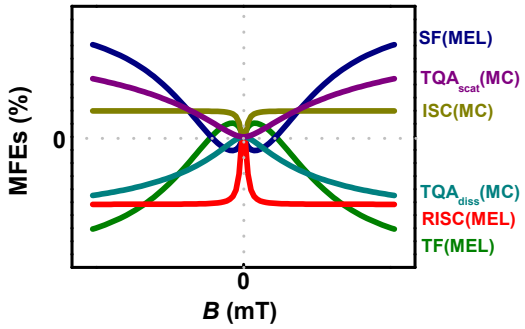

Figure S1. Schematic diagram showing fingerprint MEL curves corresponding various microscopic process (including ISC, RISC, SF, TF, and the dissociation and scattering channel of TQA process). In our previous studies,[7] we have elucidated the origin of the fingerprint MEL curves corresponding to these four microscopic mechanisms in detail.

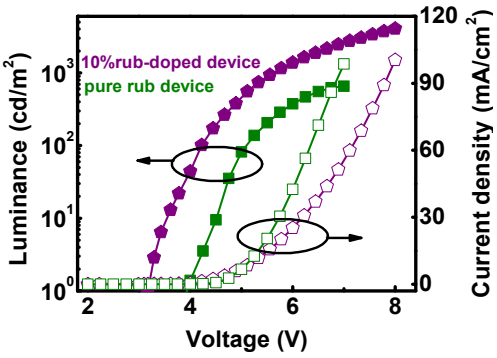

Figure S2. Luminance (*L*)-current density (*J*)-voltage (*V*) characteristic curves of 10%rubrene-doped and pure-rubrene devices.

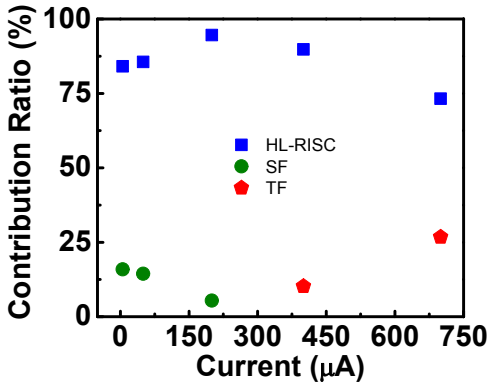

Figure S3. Current-dependent contribution ratios of three physical mechanisms including HL-RISC, TF, and SF.

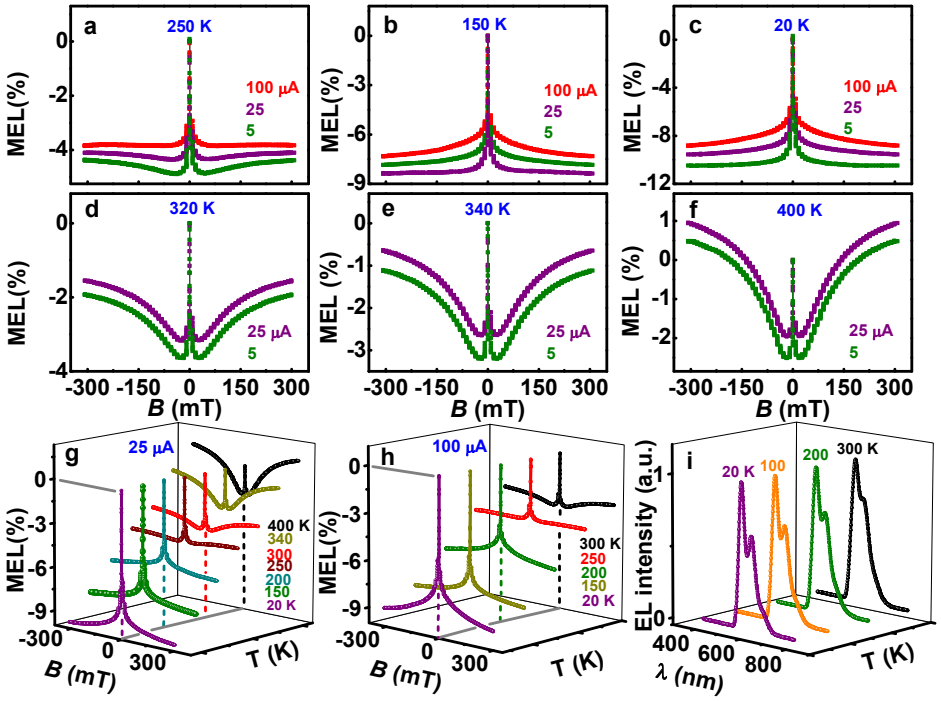

Figure S4. The MEL(*B*) response of 10%rubrene-doped OLED at various temperatures. (a) 250 K. (b) 150 K. (c) 20 K. (d) 320 K. (e) 340 K. (f) 400 K. (g) Temperature-dependent MEL(*B*) response with the current of 25 μA. (h) Temperature-dependent MEL(*B*) response with the current of 100 μA. (i) Temperature-dependent normalized EL spectra.

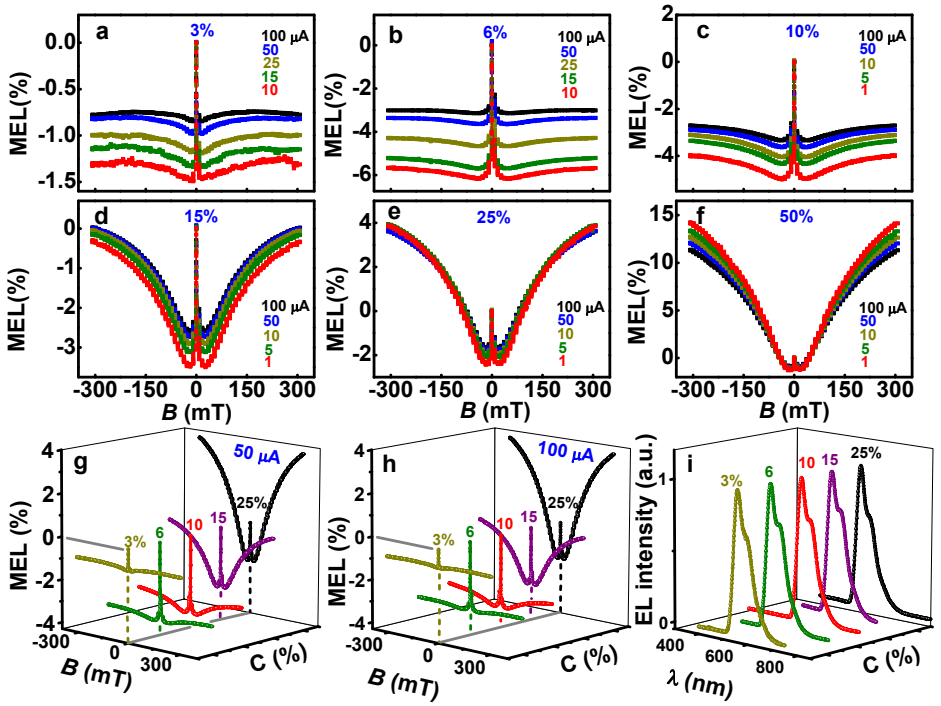

Figure S5. Current-dependent MEL(*B*) response of *x*%rubrene-doped OLEDs at various

dopant concentrations and 300 K. (a) 3%. (b) 6%. (c) 10%. (d) 15%. (e) 25%. (f) 50%. (g) Concentration-dependent MEL(*B*) response with the current of 50 μA. (h) Concentration-dependent MEL(*B*) response with the current of 100 μA. (i) Concentration-dependent normalized EL spectra.

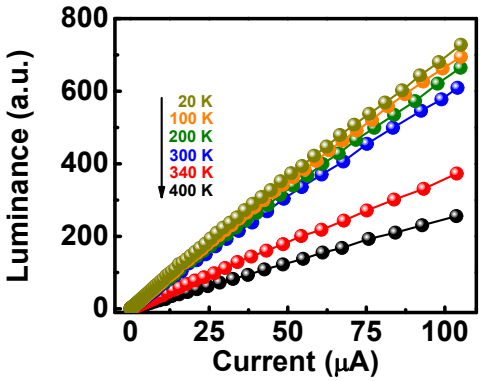

Figure S6. Luminance-current characteristic curves at different temperatures for 10%rubrene-doped device.

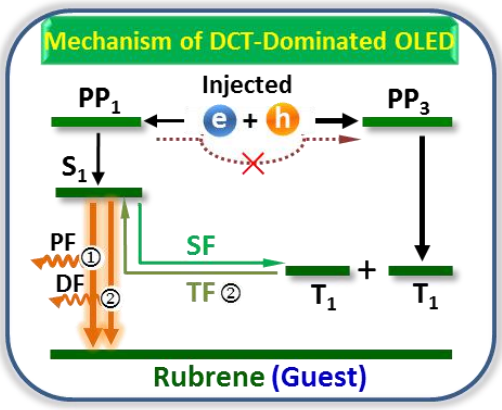

Figure S7. Schematic diagrams showing DCT-dominated mechanism in *x*%rubrene-doped OLEDs at high dopant concentration.

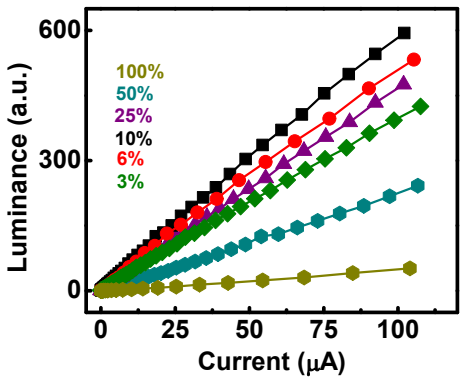

Figure S8. Luminance-current characteristic curves at different dopant concentrations for *x*%rubrene-doped device.

Reference

(1) Lee, J. H.; Lee, S.; Yoo, S. J.; Kim, K. H.; Kim, J. J. Langevin and Trap-assisted Recombination in Phosphorescent Organic Light Emitting Diodes. *Adv. Funct. Mater. 2014*, **24**, 4681−4688.

(2) Chen, P.; Lei, Y. L.; Song, Q. L.; Zhang, Y.; Liu, R.; Zhang, Q. M.; Xiong, Z. H. Magnetoelectroluminescence in Tris (8-hydroxyquinolato) Aluminum-based Organic Light-Emitting diodes Doped with Fluorescent Dyes. *Appl. Phys. Lett.* **2009**, *95*, 213304.

(3) Ramos-Ortiz, G.; Oki, Y.; Domercq, B.; Kippelen, B. Förster Energy Transfer from a Fluorescent Dye to a Phosphorescent Dopant: a Concentration and Intensity Study. *Phys. Chem. Chem. Phys.* **2002**, *4*, 4109−4114.

(4) Kim, J. W.; You, S.; Kim, N. H.; Yoon, J. A.; Cheah, K. W.; Zhu, F. R.; Kim, W. Y. Study of Sequential Dexter Energy Transfer in High Efficient Phosphorescent White Organic Light-Emitting Diodes with Single Emissive Layer. *Sci. Rep.* **2014**, *4*, 7009.

(5) Huang, W.; Mi, B. X.; Gao, Z. Q. Organic Electronics. Science Press. Beijing. 2011.

(6) Okamoto, S.; Tanaka, K.; Izumi, Y.; Adachi, H.; Yamaji, T.; Suzuki, T. Simple Measurement of Quantum Efficiency in Organic Electroluminescent Devices. *Jpn. J. Appl. Phys.* **2001**, *40*, L783–L784.

(7) Tang, X. T.; Hu, Y. Q.; Jia, W. Y.; Pan, R. H.; Deng, J. Q.; Deng, J. Q.; He, Z. H.; Xiong, Z. H. Intersystem Crossing and Triplet Fusion in Singlet-Fission-Dominated Rubrene-Based OLEDs under High Bias Current. *ACS Appl. Mater. Interfaces* **2018**, *10*, 1948−1956.